



A fragment-based approach for ligand binding affinity and selectivity for the liver X receptor beta

Lívia Barros Salum^a, Adriano Defini Andricopulo^a, Káthia Maria Honório^{b,c,*}

^a Laboratório de Química Medicinal e Computacional, Centro de Biotecnologia Molecular Estrutural, Instituto de Física de São Carlos, Universidade de São Paulo, Av. Trabalhador São-Carlense 400, 13560-970 São Carlos, SP, Brazil

^b Universidade Federal do ABC, Rua Santa Adélia, 166, Bairro Bangu, 09210-170 Santo André, SP, Brazil

^c Escola de Artes, Ciências e Humanidades, Universidade de São Paulo, Av. Arlindo Bettio, 1000, 03828-000 São Paulo, SP, Brazil

ARTICLE INFO

Article history:

Received 2 June 2011

Received in revised form

21 September 2011

Accepted 25 September 2011

Available online 7 October 2011

Keywords:

Binding affinity

Drug design

Fragment-based analysis

LXRβ

Selectivity

ABSTRACT

Selective modulation of liver X receptor beta (LXRβ) has been recognized as an important approach to prevent or reverse the atherosclerotic process. In the present work, we have developed robust conformation-independent fragment-based quantitative structure–activity and structure–selectivity relationship models for a series of quinolines and cinnolines as potent modulators of the two LXR subtypes. The generated models were then used to predict the potency of an external test set and the predicted values were in good agreement with the experimental results, indicating the potential of the models for untested compounds. The final 2D molecular recognition patterns obtained were integrated to 3D structure-based molecular modeling studies to provide useful insights into the chemical and structural determinants for increased LXRβ binding affinity and selectivity.

© 2011 Elsevier Inc. All rights reserved.

1. Introduction

Coronary heart disease (CHD) remains a leading cause of death globally. Substantial evidence indicates that the relative abundance of the different plasma lipoproteins appears to be of primary importance for the development of atherosclerosis, which is the main cause of CHD. Numerous studies have identified decreased high-density lipoprotein (HDL) and increased low-density lipoprotein (LDL) cholesterol levels as major contributors to atherosclerosis. As a consequence, many important current therapies for the treatment of CHD, including the widely used statins, are aimed at lowering LDL or increasing HDL cholesterol [1–3].

Liver X receptors (LXRs) form a subgroup of nuclear receptors called metabolic receptors, and respond to elevated levels of intracellular cholesterol by enhancing transcription of genes that control cholesterol efflux and fatty acid biosynthesis. Over the past several years, LXRs have arisen as important regulators of metabolism, being particularly important not only for the control of cholesterol, but also for the lipid and carbohydrate metabolism in insulin target tissues. In addition, LXR activity has been

demonstrated to play important roles in macrophage biology, thereby inhibiting inflammatory responses [2,4]. Several LXR agonists, such as the endogenous ligand 24(S), 25-epoxycholesterol (**a**, Fig. 1), as well as structurally distinct synthetic non-steroidal ligands, as T0901317 and GW-3965 (**b** and **c** respectively, Fig. 1) have been shown to increase the expression of several genes involved in the lipid metabolism and reverse cholesterol transport. These compounds have proven to decrease and even reverse atherosclerotic processes in multiple standard animal models. These favorable effects indicate that LXR agonists might be valuable agents in the treatment and prevention of CHD. However, the first generation of LXR agonists also activated triglyceride (TG) synthesis in the liver, provoking significant increases in serum and liver triglyceride levels, which limited the clinical utility of these compounds [4–8]. Therefore, the interest in the development of tissue-selective LXR agonists, able to retain the antiatherosclerotic activity whereas avoiding undesired lipogenic activity, has substantially increased in recent years.

There are two LXR isoforms, LXRα and LXRβ, which differ substantially in their tissue distribution: while LXRβ has a ubiquitous tissue distribution, LXRα is mainly localized in the liver, adipose tissue, intestine and macrophages. Since the LXRβ is not the dominant isoform expressed in the liver, selective LXRβ agonists, or tissue-specific LXR modulators, may have less impact on TG synthesis, but it might be effective in macrophage reverse cholesterol

* Corresponding author at: Escola de Artes, Ciências e Humanidades, Universidade de São Paulo, Av. Arlindo Bettio, 1000, 03828-000 São Paulo, SP, Brazil.
Tel.: +55 11 3091 1020.

E-mail address: kmhonorio@usp.br (K.M. Honório).

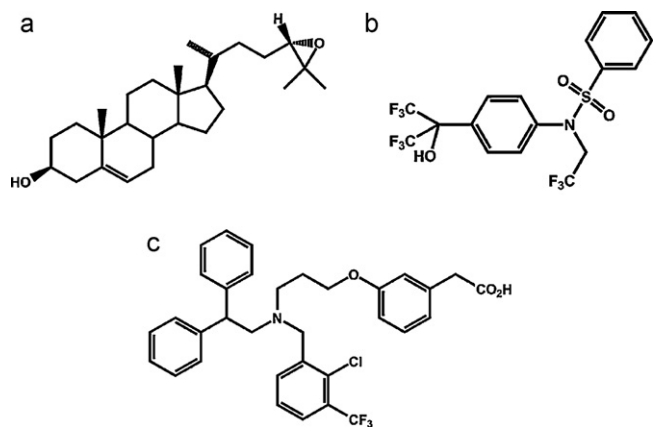


Fig. 1. Chemical structures of LXR agonists.

transport. At the same time, further experiments with wild-type and LXR α knockout mice demonstrated that selective LXR β activation is expected to reverse atherosclerosis, while having no or little effect on hepatic LXR α -dominated lipogenesis, providing a strong *in vivo* support for LXR β as an attractive target for the development of selective agonists [6,8,9].

Recently, the elucidation of crystal structures of the ligand binding domains of LXR α and LXR β isoforms, complexed with structurally distinct agonists, has provided information on the structural and functional characteristics of LXR modulation at the molecular level. The analysis of the X-ray co-crystallographic data revealed that the design of LXR β selective compounds is not trivial. The ligand-binding domains of the two isoforms share an overall 78% identity, while the ligand-binding cavities are approximately identical, differing by only one amino acid residue (i.e., LXR β Ile₂₇₇/LXR α Val₂₆₃), which is not in close contact with bound ligands. Therefore, it is not surprising that several agonists display similar affinities for both receptors [10–12]. This high resemblance in the ligand binding pockets constitutes a major challenge to the development of highly β -selective ligands. Nevertheless, subtype-selective modulators capable of accessing these different residues have been developed by using structure-based strategies, suggesting new opportunities for drug design [11–15]. Since the ligand binding pockets are very flexible, allowing structurally diverse ligands of different shapes and sizes to be accommodated, a relevant strategy toward identifying the most important structural features related to binding affinity and selectivity is combining conformation-independent methods with molecular modeling studies.

In the present study, we have employed a specialized conformation-independent fragment-based method to develop predictive quantitative structure–activity (QSAR) and structure–selectivity relationships (QSSR) for a series of quinolines and cinnolines as modulators of the two LXR subtypes. The identified molecular recognition patterns were integrated with three-dimensional molecular modeling studies to better understand the chemical and structural features required for LXR binding affinity and subtype-selectivity.

2. Methodology

2.1. Data set

The data set used for the QSAR and molecular modeling studies encloses 62 quinolines and cinnolines as modulators of the LXR α and LXR β subtypes, which were synthesized and evaluated by the same group [12–15]. The binding affinities (IC₅₀) were measured under the same experimental conditions, a fundamental

requirement for successful QSAR analyses. The β pIC₅₀ values, $-\log$ IC₅₀ for LXR β , were used as dependent variables in the QSAR investigations. The selectivity parameter $\log S$, $\log(\alpha\text{IC}_{50}/\beta\text{IC}_{50})$, was used for the QSSR models [16]. Representative chemical structures and their corresponding β pIC₅₀ and $\log S$ values are listed in Table 1. The complete data set is listed in Supplementary Table 1.

2.2. Computational methods

Hologram QSAR (HQSAR), QSSR (HQSSR) and molecular modeling analyses, calculations, and visualizations were performed using the SYBYL 8.0 (Tripos Inc., St. Louis, USA), GOLD 3.1 (Cambridge Crystallographic Data Centre, Cambridge, UK) and Pymol (Delano Software) running Red Hat Enterprise Linux workstations. The 3D structures of the LXR modulators were constructed using the standard geometric parameters of SYBYL 8.0. Carboxylic acids were modeled in their deprotonated states. Each single optimized conformation of each molecule in the data set was energy minimized employing the Tripos force field and the Gasteiger–Hückel charges were calculated. Non-supervised hierarchical cluster analyses (HCA) performed within SYBYL 8.0 were used with the aim to select the training and test compound sets.

2.3. Hologram QSAR and QSSR models

Predictive QSAR and QSSR models were constructed using the HQSAR approach as previously described in several drug design studies [17–22]. Briefly, molecular holograms were generated for each molecule of the data set, using different combinations of parameters concerning hologram generation (e.g., hologram length, fragment size, and fragment distinction), as schematically depicted in Fig. 2. The statistical coefficients obtained for the different HQSAR models were employed to determine the combinations of parameters that best describe the chemical space of the training set compounds. Accordingly, several combinations of fragment distinction parameters were considered during the QSAR modeling runs, given that the holograms were generated using distinct combinations of atoms (A), bonds (B), connections (C), hydrogen atoms (H), chirality (Ch), and donor and acceptor (DA) as fragment distinctions. The HQSAR and HQSSR analyses were performed by screening the 12 default series of hologram length values ranging from 53 to 401 bins using distinct fragment sizes (2–5, 3–6, 4–7, 5–8 and 6–9 atoms). The patterns of fragment counts were then related to the dependent variables using the partial least squares (PLS) regression analyses to derive the HQSAR and HQSSR models. Cross-validation procedures (q^2 leave-one-out, q^2_{LOO} and leave-many-out, q^2_{LMO} with either 10 or 5 randomly selected groups) were used to determine the number of components that yielded optimally predictive models and to assess the stability and statistical significance of the models [17]. The patterns of fragment counts related to increasing LXR β binding affinity and selectivity were integrated with the three-dimensional molecular modeling studies [23–25].

2.4. Molecular modeling studies

To explore ligand-binding conformations and molecular interactions contributing to the binding affinity and selectivity of quinolines and cinnolines to LXR β , docking and scoring protocols were used as implemented in GOLD 3.1. The crystal structure of LXR β in complex with compound 5 (Table 1) was used for the docking studies, following the removal of the ligand and water molecules [14]. Hydrogen atoms were added in standard geometry and the structure was energy minimized with the non-hydrogen atoms constrained. Histidine and glutamine residues in the binding site were manually checked for possible flipped orientation, protonation, and tautomeric states. The docking site within LXR β

Table 1Representative chemical structures and the associated βpIC_{50} and $\log S$ values used for the QSAR studies.

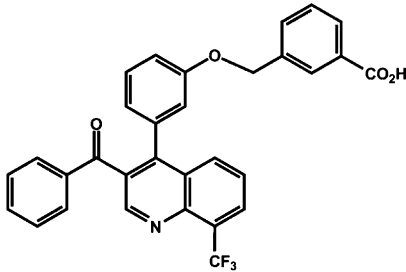
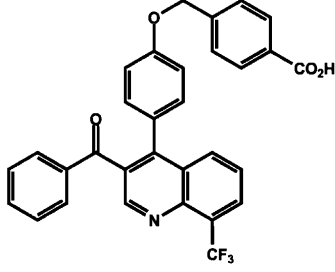
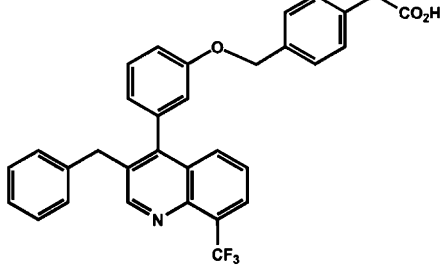
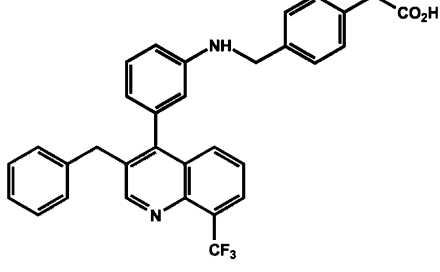
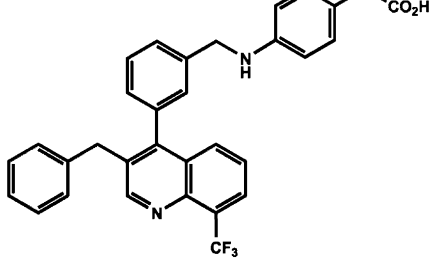
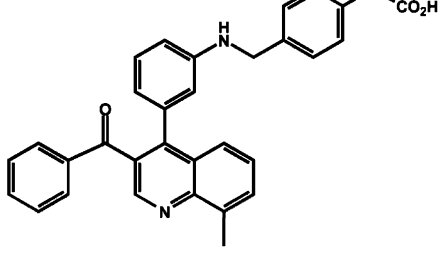
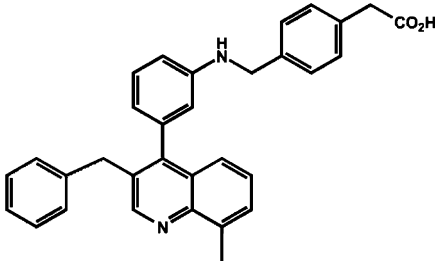
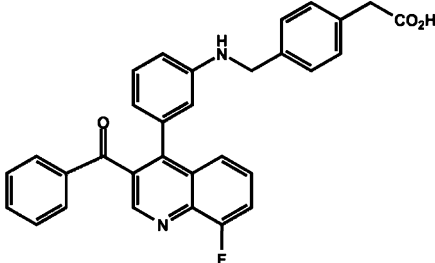
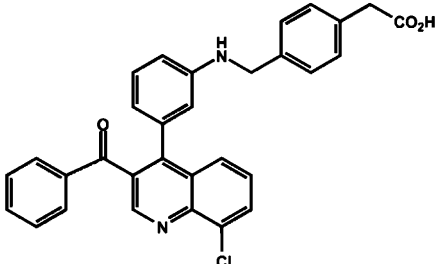
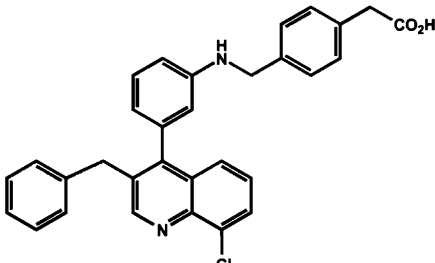
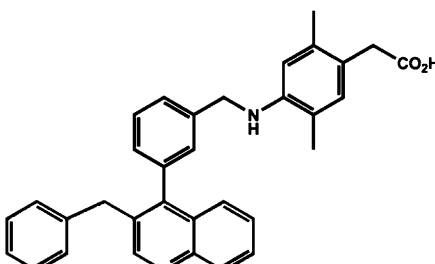
Compound	Structure	βpIC_{50}	$\log S$
2		5.99	0.26
3		5.56	-0.58
5		8.68	0.66
6		8.72	0.60
7		8.15	0.83
10		8.26	0.51

Table 1 (Continued)

Compound	Structure	β pIC ₅₀	log S
11		8.30	0.62
12		7.77	0.79
13		8.57	0.52
14		8.85	0.55
28		8.7	1.02

was defined by the ligand in the structure. The GoldScore scoring function was employed, and the search efficiency was set to the maximum (200%). Each ligand was docked 20 times with early termination allowed when the 3 best ranked solutions were within 1.5 Å RMSD. Only the top-ranked conformations were considered for the molecular modeling studies. X-ray structures of LXR α (PDB IDs 1ULH, 2ACL and 3FC6) and LXR β (PDB IDs 1P8D, 1PQ6, 1PQ9 and the structure in complex with compound **5**), which are in complex with structurally diverse ligands, were used to compare the

proposed binding models of the ligands disclosed in Table 1. The structure in complex with quinoline **5** was chosen as a template and all other X-ray structures were subject to a structural alignment in Pymol.

2.5. Molecular fields

Molecular hydrophobic interaction energies were calculated as implemented in CoMSIA. The docking conformations of the ligands

Table 1 (Continued)

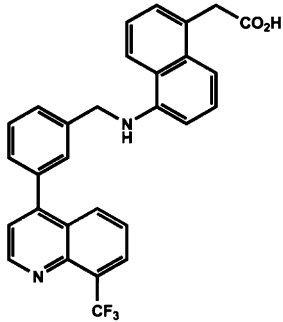
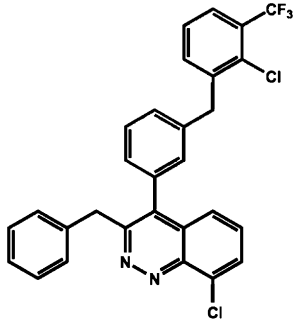
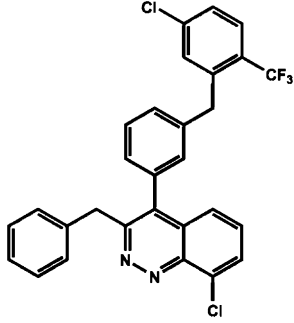
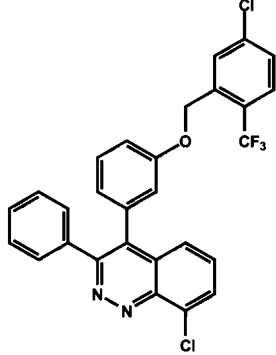
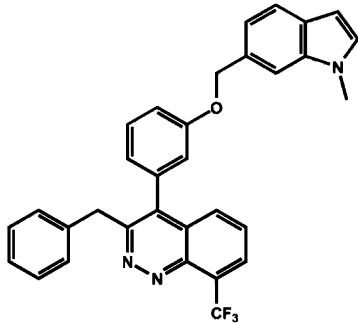
Compound	Structure	βpIC_{50}	log S
34		7.82	1.70
36		7.62	1.54
38		7.07	1.33
42		7.19	0.71
47		7.85	1.85

Table 1 (Continued)

Compound	Structure	βpIC_{50}	log S
48		7.47	1.62
51		6.00	0.00
62		8.00	0.79

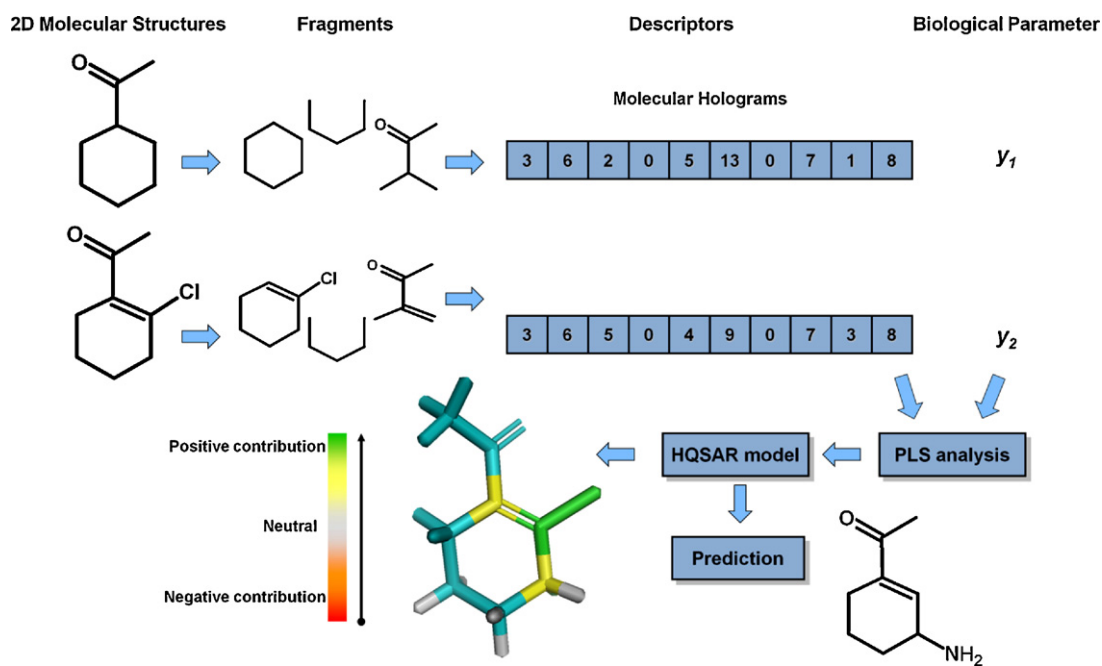


Fig. 2. Generation of molecular holograms and HQSAR models.

2, **3**, **14** and **47** were positioned in a 3D grid box embedding all analogs with a margin of 4 Å in each direction. CoMSIA fields were computed for the hydrophobic physicochemical properties using a probe of charge +1, a radius of 1, hydrophobicity of +1 and an attenuation factor of 0.3 for the Gaussian distance-dependent function. The fields were visualized in the same limits of favorable and unfavorable hydrophobic interactions (−3 and 40 kcal/mol, respectively) [26].

3. Results and discussion

3.1. Data set characterization

QSAR and QSSR models were derived for a series of 62 LXR β modulators for which the binding affinities for both LXR subtypes (as measured by IC_{50}) were determined under the same experimental conditions [12–15] (Supplementary Table 1). The IC_{50} values for LXR β were converted to the corresponding βpIC_{50} ($-\log IC_{50}$) and used as dependent variables in the QSAR investigations. The selectivity parameter was defined as the ratio of the binding affinities of the isoforms α and β ($\alpha IC_{50}/\beta IC_{50}$), whose values were then converted to the corresponding $\log S$. Representative chemical structures and their corresponding βpIC_{50} and $\log S$ values are listed in Table 1. The compounds of the data set are structurally represented for 4-phenylquinolines and 4-phenylcinnolines, which present variations at positions C8 (R^1) and C3 (R^2) of the respective quinoline and cinnoline systems, as well as in the *meta* (R^3) or *para* (R^4) positions of the attached phenyl ring, as depicted in Fig. 3. The binding affinity values (βIC_{50}) for LXR β are distributed over more than 3 orders of magnitude, varying from 1.4 to 2740 nM. The selectivity parameter varies from 0.26 to 71-fold (a factor of 275 times).

The generation of reliable statistical models is dependent on the creation of appropriate training and test sets. Therefore, from the original data set of 62 LXR modulators, 50 ligands were selected as members of the training set for model construction (**1–50**, Supplementary Table 1) and the remaining 12 compounds (**51–62**, Supplementary Table 1) were defined as members of the test set for external validation of the models. HCA technique was used to guide an appropriate compound selection. Consequently, training and test sets were selected in such a way that structurally diverse molecules, possessing activities of a wide range, were included in both sets.

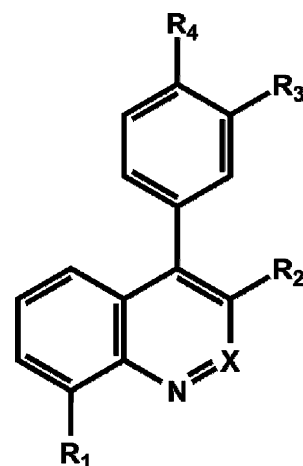


Fig. 3. General 4-phenylquinoline/4-phenylcinnoline scaffold of the LXR β modulators displaying regions where substitutions are responsible for differences in binding affinity and selectivity.

3.2. HQSAR and HQSSR analyses

As the HQSAR method is capable of incorporating 3D structural information (e.g., hybridization and chirality) into the generated molecular holograms without requiring explicit 3D information for the ligands (e.g., determination of 3D structure, putative binding conformations, and molecular alignment) [23–25], we have selected this approach to study the highly flexible and complex system consisting of LXR β and its modulators. In this context, several combinations of atoms (A), bonds (B), connections (C), hydrogen atoms (H), chirality (Ch), and donor and acceptor (DA) were employed as fragment distinctions for obtaining the molecular fragments during the HQSAR modeling runs. The influence of the fragment size in the generation of the molecular holograms, and consequently in the HQSAR and HQSSR statistical parameters, was also investigated [17]. The patterns of fragment counts from the training set compounds were related to the experimental values of βpIC_{50} and $\log S$ using the PLS analyses. The parameters that provided the best HQSAR and HQSSR models are shown in Table 2.

From Table 2, it can be noted that significant statistical coefficients were obtained when A/B/C was used as fragment distinction for both LXR β -binding affinity and selectivity models ($r^2 = 0.82$ and $q^2 = 0.65$, with 5 principal components for binding affinity; and $r^2 = 0.84$ and $q^2 = 0.69$, with 4 principal components for selectivity). Interestingly, although the number of optimal principal

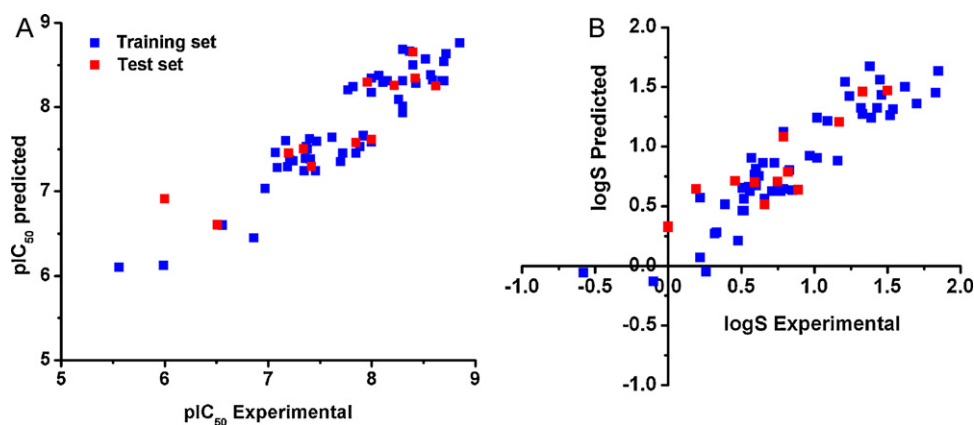


Fig. 4. (A) Plot of predicted values of βpIC_{50} versus the corresponding experimental values for the 50 training set compounds (blue squares) and the 12 test set compounds (red squares). (B) Predicted values of $\log S$ versus the corresponding experimental values for the 50 training set compounds (blue squares) and the 12 test set compounds (red squares). (For interpretation of the references to color in this figure legend, the reader is referred to the web version of the article.)

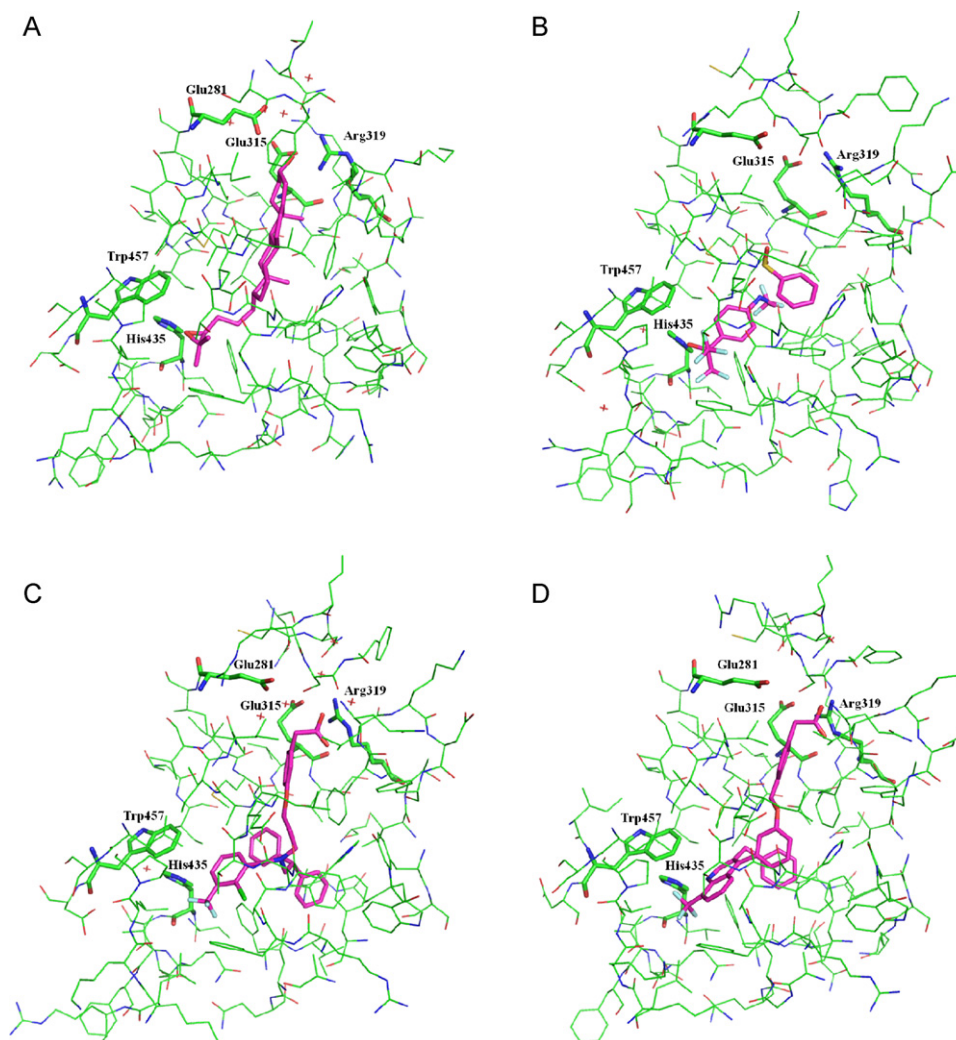


Fig. 5. Binding modes of compounds: (A) **a**, (B) **b**, (C) **c** and (D) **5**, showing the main amino acid residues that form the ligand binding pocket of LXRβ. The ligands are shown in sticks. Hydrogen atoms have been eliminated for clarity. PDB IDs: (A) 1P8D, (B) 1PQ6 and (C) 1PQ9, respectively. Key residues in the binding site are identified by the residue number and are highlighted in sticks.

components is different for these models, both were generated by using a combination of reasonably short hologram lengths (61 and 71, respectively) and fragment sizes (2–5 atoms). In the other models, while the donor/acceptor characteristic was important to describe the binding affinity for LXRβ, non-polar hydrogen atoms were more important in the generation of statistically significant models for selectivity.

Table 2
HQSSAR and HQSSR models for a series of LXR modulators.

Model	Statistical Parameters					
	q_{Loo}^2	r^2	HL	N	Size ^a	r_{pred}^2
Binding affinity						
A/B/C	0.65	0.82	61	5	2–5	0.59
A/B/C/DA	0.63	0.86	401	5	4–7	0.79
Selectivity						
A/B/C	0.69	0.84	71	4	2–5	0.74
A/B/C/H	0.69	0.92	151	6	5–8	0.56

q_{Loo}^2 , leave-one-out cross-validated correlation coefficient; r^2 , non-cross-validated correlation coefficient; HL, hologram length; N, optimal number of components; Size, fragment size; r_{pred}^2 , predictive correlation coefficient.

^a Fragment size employed in this analysis: 2–5, 3–6, 4–7, 5–8, 6–9 and 7–10.

The predictive power of the HQSSAR and HQSSR models was assessed by predicting βpIC_{50} and $\log S$ values for the test set compounds (**51–62**, Supplementary Table 1). The predictive r^2 (r_{pred}^2) coefficients for the 4 models are shown in Table 2. As it can be seen, while the hydrogen bond parameters were related to an increase in the ability of correctly predicting the binding affinity values for LXRβ, the simplest model (using A/B/C as parameters of fragment distinction) was the most reliable for predicting β -selectivity. The results of the external validation process can be visualized in Fig. 4 and are listed in Table 3. The predicted values fall close to the experimental βpIC_{50} and $\log S$, deviating by less than one log unity. From the low residual values, it can be seen that the constructed HQSSAR and HQSSR models obtained are reliable and can be used in further studies intended to comprehend the molecular determinants for LXRβ binding affinity and selectivity.

3.3. Chemical determinants for LXRβ binding affinity

The LXR modulators can be considered as a collection of molecular fragments having chemical groups particularly connected and positioned to establish intermolecular interactions with complementary groups in the protein binding pocket. Therefore, the patterns of substructural fragments derived from the predicted HQSSAR and HQSSR models could be related to the selective

molecular interactions in the chemical environment of the LXR β binding pocket, providing important hints about what molecular fragments are directly related to the biological properties [17,18,23,24,27]. This can be accomplished through a meticulous examination of the structural fragments incorporated to the hologram-based QSAR models. A color system is employed by the HQSAR module implemented in SYBYL 8.0: the colors at the red end of the spectrum (red, red orange and orange) indicate poor contributions, whereas colors at the green end (yellow, green blue and green) reflect favorable contributions (atoms with intermediate contributions are colored white) [23–25].

Fig. 5 shows the crystallographic binding mode of compounds **a**, **b**, **c** and **5** into the binding cavity of LXR β , revealing a number of important molecular characteristics [10,14,28]. In spite of their chemical diversity, compounds **a**, **b**, **c** and **5** partially superpose in the flexible LXR β binding site. For instance, compound **5** occupies the binding pocket in a similar way to that of the cholesterol derivative **a** and the tertiary amine **c**, establishing polar interactions with Arg319 and His435. The negative carboxylate of Glu315 and the positively charged Arg319 group, which are hydrogen-bonded themselves, are positioned in such a way that Arg319 sets up an important salt bridge with the negatively charged 2-phenylacetate substituent of compound **5**, which is sufficiently far from the negative charge of Glu315. Different from compound **a**, the quinoline derivative **5** exploits an additional hydrophobic region delimited by the side chains of Phe340, Phe454, Leu345 and Ile353, similarly to compound **c**. Moreover, electrostatic interactions with His435 and Trp457 are distinct for modulators **a**, **b** and **5**. The methoxyphenyl system attached to the 4-phenylquinoline system of **5** tightly fits to the pocket surrounded by Phe329 and Ser278. The same region is occupied by the rigid sterol system in **a** and the ethoxybenzene group in **b**. However, it can be observed that there is room available for more substituents, which could be linked to the position *meta* of the terminal aromatic ring *para*-substituted or to the linked methylene group of the terminal acetate in compound **5**.

Fig. 6 displays the individual atomic contributions for the representative compounds having high binding affinities for LXR β (compounds **6**, **11**, **14** and **28**, Table 1) as well as the HQSAR contribution maps for a single compound with low binding affinity for this nuclear receptor (compound **2**, Table 1). The maximum common substructure for the modulators is shown in blue. The proposed binding conformations for each of these compounds into the LXR β ligand binding cavity, as selected from the docking studies, are also depicted. Furthermore, hydrophobic interaction fields, as calculated with CoMSIA, are shown in Fig. 6 for compounds **14** and **2** (Table 1).

A comparison of the contribution maps and corresponding proposed binding conformations revealed the importance of the negatively charged acetate group, which interacts with Arg319 through an electrostatic interaction (Fig. 6A and D). As shown in the maps, the acid group has to be located at the *meta* position (and not in the *para* position) of the phenylacetate terminal to positively contribute to the binding affinity (compare the most potent compounds with compound **3**). Although negatively charged groups at the *meta* position are related to an increase in the binding affinity, the benzoate substituent in **2** is not correctly positioned towards Arg319 and, therefore, represents a negative contribution to this property (Fig. 6E), similar to the ester derivative **51**. Furthermore, as shown in Fig. 7, the hydrophilic character related to the acid substituent is more pronounced for the acetate derivative **14**, having the highest binding affinity, when compared to the benzoate analogue **2**, presenting low binding affinity. Therefore, a methylene group was found to be the optimal link between the terminal aromatic ring and the negatively charged end. Moreover, only small substituents (hydrogen atom or methyl group) are tolerated at the *ortho* position of the terminal phenyl ring

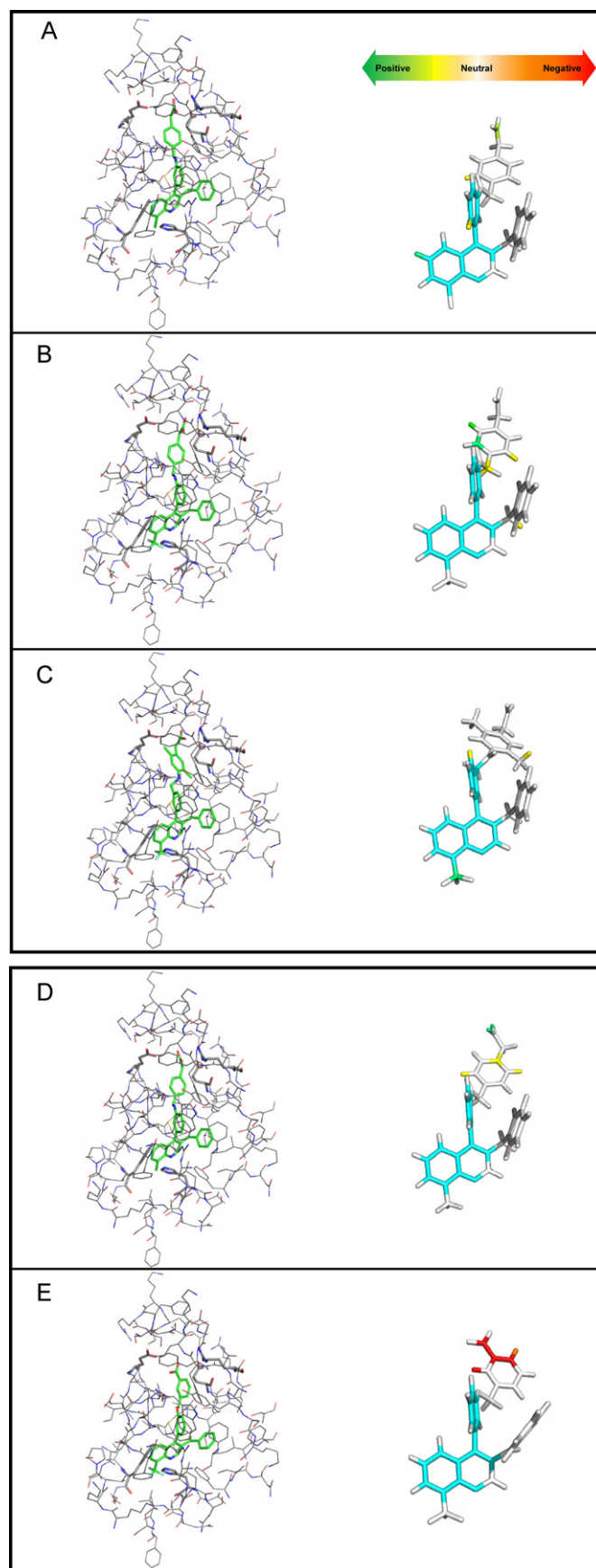
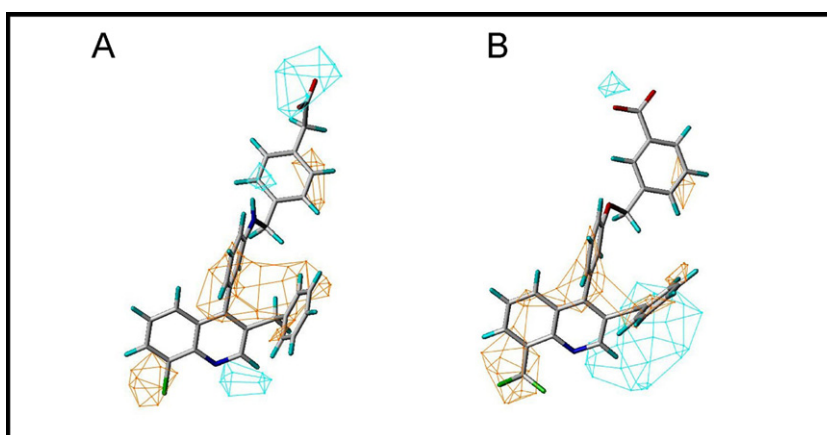


Fig. 6. Structural features required for binding affinity and biological activity, as highlighted by the fragment-based HQSAR models. Contribution maps and proposed 3D binding conformations into the LXR β ligand binding pocket for compounds (A) **14**, (B) **6**, (C) **28**, (D) **11** and (E) **2**.

Table 3Experimental and predicted values of βpIC_{50} and $\log S$ for the LXR modulators employed in the HQSAR and HQSSR studies.

Compound	Experimental βpIC_{50}	Predicted βpIC_{50}	Residual ^a βpIC_{50}	Experimental $\log S$	Predicted $\log S$	Residual ^a $\log S$
51	6.00	6.91	0.91	0.00	0.33	0.33
52	8.62	8.25	−0.37	0.46	0.71	0.25
53	8.22	8.26	0.04	0.75	0.70	−0.05
54	8.42	8.34	−0.08	0.66	0.51	−0.15
55	6.51	6.60	0.09	0.19	0.64	0.45
56	8.40	8.65	0.25	0.89	0.63	−0.26
57	7.96	8.29	0.33	1.17	1.21	0.04
58	7.34	7.50	0.16	0.59	0.70	0.11
59	7.85	7.58	−0.27	0.82	0.79	−0.03
60	7.42	7.29	−0.13	1.50	1.47	−0.03
61	7.20	7.45	0.25	1.33	1.46	0.13
62	8.00	7.61	−0.39	0.79	1.08	0.29

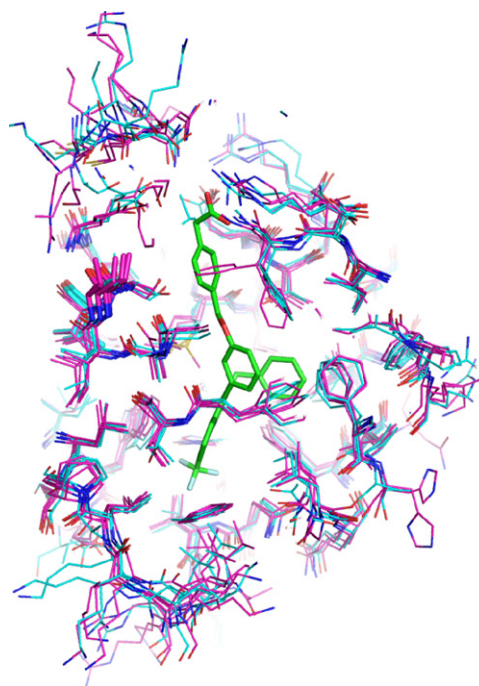
^a Difference between the logarithms of the predicted and experimental values.**Fig. 7.** Isocontours of hydrophobic properties based on CoMSIA (contour level at −3, yellow and 40, cyan kcal/mol) for compounds (A) **14** and (B) **2**.

(Fig. 6B–D), reinforcing that this ring is tightly fitted in the binding pocket.

The importance of groups such as trifluoromethyl at R^1 (or C8) and the methyl or carbonyl linker at R^2 (or C3) is also evidenced by the generated HQSAR patterns (see compounds **10** and **12**, Fig. 5B and C). The hydrophobic nature of the R^1 group is depicted in Fig. 7, which also shows that the methyl and carbonyl groups at R^2 are associated with opposite characters, hydrophobic and hydrophilic, respectively. Furthermore, the positive contribution of the linker benzylamine or benzylether (compare compounds **5**, **6** and **7**) is revealed in Fig. 6B.

3.4. Chemical determinants for LXR β selectivity

Although compound **5** demonstrates high binding affinity for LXR β , its selectivity is rather modest (Fig. 4). In order to understand the structural determinants for LXR β selectivity, we have analyzed the structural characteristics contributing positively to the HQSSR models. The ligand-based analyses of the 2D features related to β -selectivity were integrated with 3D molecular modeling studies into the ligand binding cavities of the known crystal structures of LXR α and LXR β isoforms, obtained in complex with structurally diverse ligands, with the aim of taking into account the structural flexibility of the receptors. The structures of LXR α (PDB IDs 1ULH, 2ACL and 3FC6) and LXR β (PDB IDs 1P8D, 1PQ6 and 1PQ9) were rigidly superposed on the structure in complex with quinoline **5** (used as template), with RMSD less than 1 Å, even in the cases where different LXR isoforms were used, indicating that the structures are very similar. In fact, the ligand-binding domains of the LXR α and LXR β isoforms share a high identity (78%), and the ligand-binding cavities are nearly identical – they differ only by one

**Fig. 8.** Differences in the mode of interaction of quinoline **5** with LXR α (cyan, PDB IDs 1UHL, 2ACL and 3FC6) and LXR β (pink, PDB IDs 1P8D, 1PQ6 and PQ9). The ligand and the different residues, Val263 in LXR α and Ile277 in LXR β are shown in sticks. (For interpretation of the references to color in this figure legend, the reader is referred to the web version of the article.)

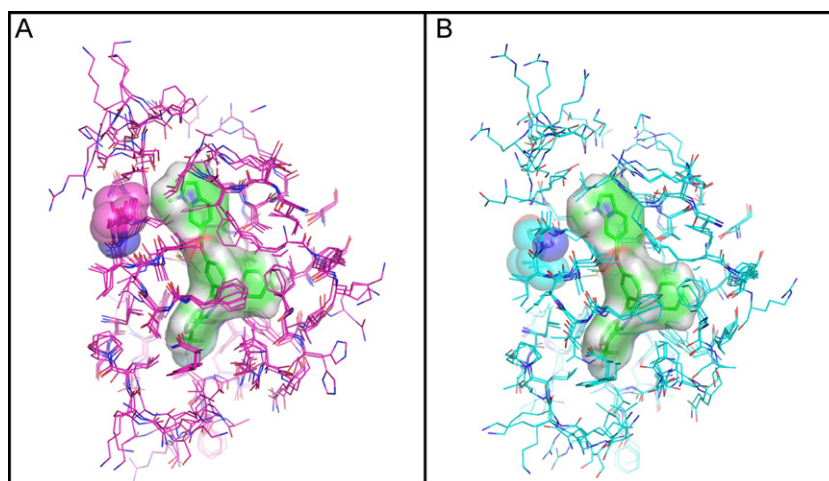


Fig. 9. Differences in the interaction mode of the most selective cinnoline (**47**) in the binding cavities of LXR α and LXR β , as proposed by the molecular modeling studies. (A) LXR β binding pocket – amino acid residues of the different crystallographic structures of LXR β (PDB IDs 1P8D, 1PQ6 and 1PQ9) and the surface of Ile277 are shown in pink. (B) LXR α binding pocket – amino acid residues of the different crystallographic structures (PDB IDs 1ULH, 2ACL and 3FC6) and the surface of Val263 are shown in cyan. (For interpretation of the references to color in this figure legend, the reader is referred to the web version of the article.)

amino acid residue (LXR β Ile₂₇₇/LXR α Val₂₆₃), which is not in close contact with the ligands. As it can be seen in Fig. 8, which depicts the superposition of LXR α and LXR β binding cavities, this dissimilar residue is located in the neighborhood of the delimited region in the cavity that interacts with the tightly positioned terminal aromatic ring of quinoline **5**, as previously discussed.

The proposed binding conformation of the most β -selective cinnoline (**47**) into the LXR β binding cavity, displayed in Fig. 9, shows the main observed differences between the two LXR isoforms. It is possible to note that the bulkier side chain of Ile277 in LXR β , which is replaced for Val263 in LXR α , is in close contact with the fused ring system of compound **47** and, therefore, van der Waals interactions might represent the principal contribution to the selectivity of **47**. An extensive and important hydrophobic area surrounding the methyl indole substituent can be, therefore, related to the selective interactions presented by cinnoline **47** (Fig. 10). A smaller hydrophobic area corresponding to the benzoate substituent of **3** is also shown in Fig. 10.

Fig. 11 shows the HQSSR individual atomic contributions for the most selective compounds (quinoline **34** and cinnolines **47** and **48**, Table 1), for a modulator with only modest selectivity (compound **62**, Table 1) and for a non-selective (moderated α -selective) ligand (quinoline **3**, Table 1). The proposed binding conformations of these compounds into the LXR β cavity along with the differences in the pockets of LXR α and LXR β are also depicted. As it can be

observed, larger and bulkier groups at the *meta* position of the 4-phenylquinoline (compound **34**) or 4-phenylcinnoline (compounds **47** and **48**) systems, as well as other ring systems or substituted analogs (also consider compound **36**), positively contribute to β -selectivity, possibly because of the interaction with Ile227 of LXR β in detriment of Val263 in LXR α (Figs. 10 and 11A–D). It is also worth noting that the linker benzylamine (or benzylether) is also related to increased binding affinity and β -selectivity. Moreover, although the binding affinity for LXR β is positively affected by the presence of the trifluoromethyl substituent (Fig. 5), the same is not the case for the selectivity for this isoform (compare quinoline derivatives **10**, **12** and **13**).

The importance of aliphatic alkyl groups in R₂ (or C₃) can also be observed, because a phenyl substituent at this position, directly linked to the 4-phenylquinoline or 4-phenylcinnoline core, contributed negatively to β -selectivity while not being directly involved with a reduction in the binding affinity for LXR β . A comparison of compounds **38** and **42** revealed that although they have similar binding affinities for LXR β , the compound presenting the methyl spacer in R₂ was considerably more selective. On one hand, the subpocket of interaction of the substituents in R₂ is hydrophobic and, therefore, lipophilic groups are related to a higher binding affinity for LXR β . On the other hand, the phenyl substituent directly connected to this position of the quinoline/cinnoline scaffold is related to a higher binding affinity for LXR α , which results

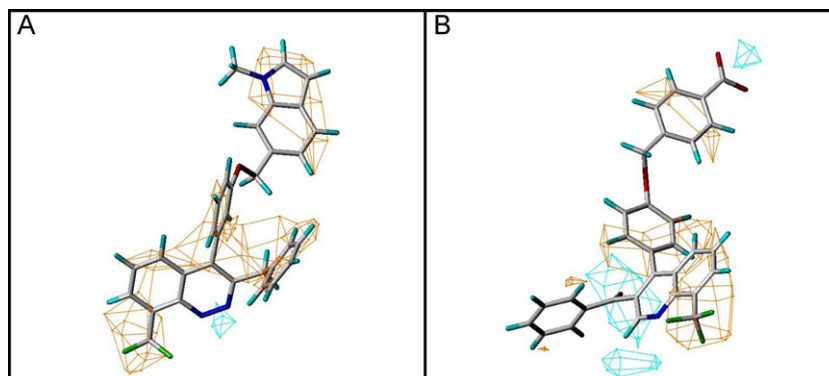


Fig. 10. Isocontours of hydrophobic properties based on CoMSIA (contour level at –3, yellow and 40, cyan kcal/mol) for compounds (A) **47** and (B) **3**. (For interpretation of the references to color in this figure legend, the reader is referred to the web version of the article.)

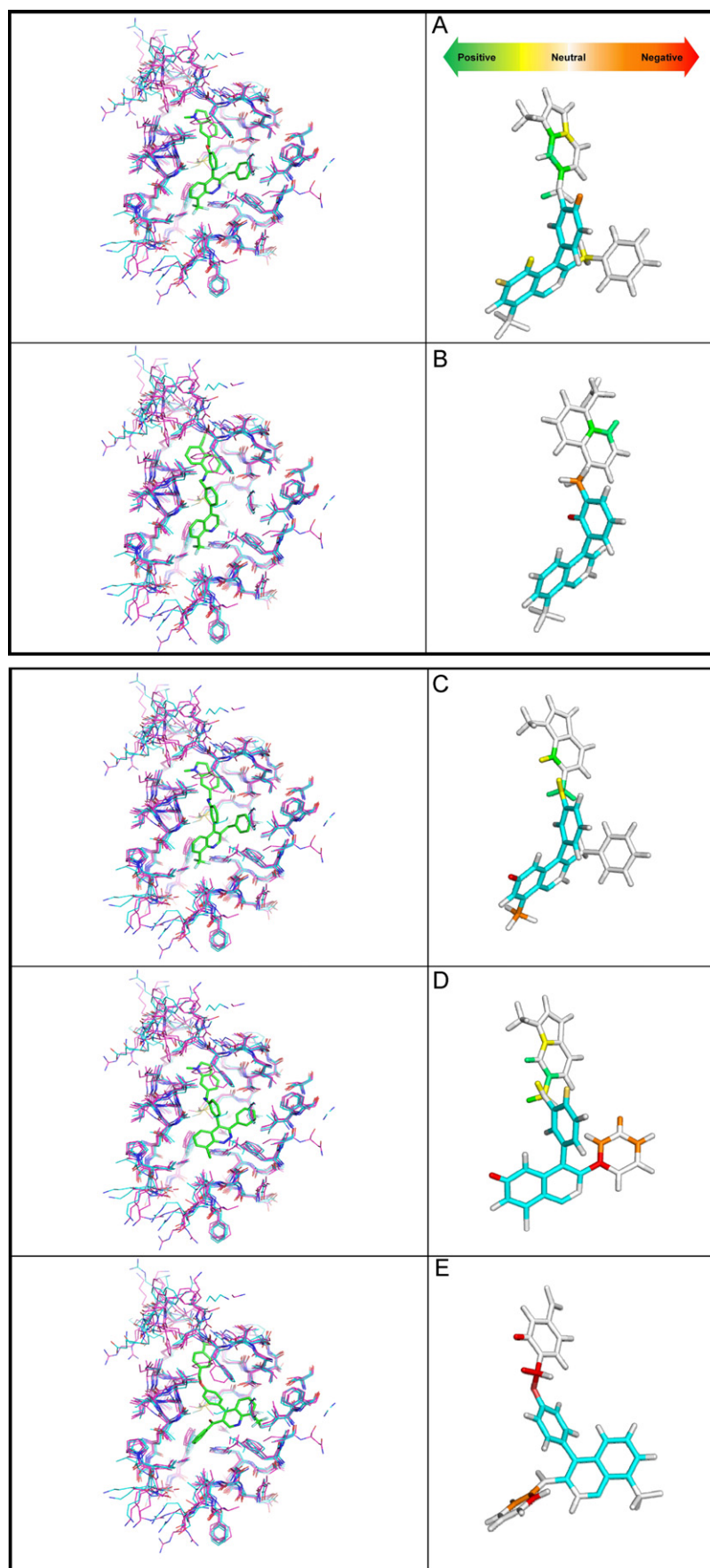


Fig. 11. Structural requirements for β -selectivity, as highlighted by the fragment-based HQSSR models. Contribution maps and proposed binding models into the LXR α (cyan) and LXR β (pink) binding cavities for compounds (A) 47, (B) 34, (C) 48, (D) 62 and (E) 3. (For interpretation of the references to color in this figure legend, the reader is referred to the web version of the article.)

in a decreasing β -selectivity (also consider compound **18**). In general, bulkier groups in R¹ (or C₈) are associated with LXR α binding affinity, while electronegative groups seem to be favored for LXR β . Furthermore, the phenyl substituent linked to the 4-phenylquinoline/cinnoline scaffold, when in the position *para* position with respect to the benzylamine or benzylether linker, also represents a negative contribution to selectivity (Fig. 11E). Finally, the carbonyl group in R² (C₃) leads to a decrease in β -selectivity (Fig. 11E), although this effect is less significant than the effect of the directly linked phenyl group (compare with compound **62**).

4. Conclusions

The interest in the development of tissue-selective LXR agonists, while retaining the antiatherosclerotic activity and avoiding undesired lipogenic activity, has substantially increased in recent years. In this study, the integration of the 2D fragment-based HQSAR and HQSSR models with 3D structure-based molecular modeling investigations allowed the identification of chemical and structural characteristics related to binding affinity and selectivity for LXR β . The 2D contribution maps along with the structural studies provided unique insight into the molecular determinants for the biological activity of this series of LXR modulators, emphasizing important fragments that can be modified in order to generate new LXR β modulators with improved properties.

Acknowledgments

We gratefully acknowledge financial support from FAPESP (The State of São Paulo Research Foundation), CNPq (The National Council for Scientific and Technological Development) and CAPES (Coordination for the Improvement of High Education Personnel), Brazil. We thank Dr. Baihua Hu and Dr. Rayomand Unwalla for kindly and promptly providing the PDB coordinates of LXR β in complex with WAY-254011 (compound **5**, Table 1).

Appendix A. Supplementary data

Supplementary data associated with this article can be found, in the online version, at doi:10.1016/j.jmgm.2011.09.007.

References

- [1] R. Ross, Mechanisms of disease – atherosclerosis – an inflammatory disease, *N. Engl. J. Med.* 340 (1999) 115–126.
- [2] C.K. Glass, J.L. Witztum, Atherosclerosis: the road ahead, *Cell* 104 (2001) 503–516.
- [3] M.E. Brousseau, Emerging role of high-density lipoprotein in the prevention of cardiovascular disease, *Drug Discov. Today* 10 (2005) 1095–1101.
- [4] J.L. Collins, Therapeutic opportunities for liver X receptor modulators, *Curr. Opin. Drug Discov. Dev.* 7 (2004) 692–702.
- [5] M. Jaye, LXR agonists for the treatment of atherosclerosis, *Curr. Opin. Invest. Drugs* 4 (2003) 1053–1058.
- [6] D.J. Bennett, E.L. Carswell, A.J. Cooke, A.S. Edwards, O. Nimz, Design, structure activity relationships and X-ray co-crystallography of non-steroidal LXR agonists, *Curr. Med. Chem.* 15 (2008) 195–209.
- [7] N. Mitro, P.A. Mak, L. Vatgas, C. Godio, E. Hampton, V. Molteni, A. Kreusch, E. Saez, The nuclear receptor LXR is a glucose sensor, *Nature* 445 (2007) 219–223.
- [8] B. Miao, S. Zondlo, S. Gibbs, D. Cromley, V.P. Hosagrahara, T.G. Kirchgessner, J. Billheimer, R. Mukherjee, Raising HDL cholesterol without inducing hepatic steatosis and hypertriglyceridemia by a selective LXR modulator, *J. Lipid Res.* 45 (2004) 1410–1417.
- [9] E.M. Quinet, D.A. Savio, A.R. Halpern, L. Chen, G.U. Schuster, J.A. Gustafsson, M.D. Basso, P. Nambi, Liver X receptor (LXR)-beta regulation in LXRalpha-deficient mice: implications for therapeutic targeting, *Mol. Pharmacol.* 70 (2006) 1340–1349.
- [10] M. Faernegardh, T. Bonn, S. Sun, J. Ljunggren, H. Ahola, A. Wilhelmsson, J.A. Gustafsson, M. Carlquist, The three-dimensional structure of the liver X receptor β reveals a flexible ligand-binding pocket that can accommodate fundamentally different ligands, *J. Biol. Chem.* 278 (2003) 38821–38828.
- [11] H. Ratni, M.B. Wright, Recent progress in liver X receptor-selective modulators, *Curr. Opin. Drug Discov. Dev.* 13 (2010) 403–413.
- [12] B. Hu, M. Collini, R. Unwalla, C. Miller, R. Singhaus, E. Quinet, D. Savio, A. Halpern, M. Basso, J. Keith, V. Clerin, L. Chen, C. Resmini, Q.Y. Liu, I. Feingold, C. Huseilton, F. Azam, M. Farnegardh, C. Enroth, T. Bonn, A. Goos-Nilsson, A. Wilhelmsson, P. Nambi, J. Wrobel, Discovery of phenyl acetic acid substituted quinolines as novel liver X receptor agonists for the treatment of atherosclerosis, *J. Med. Chem.* 49 (2006) 6151–6154.
- [13] B. Hu, J. Jetter, D. Kaufman, R. Singhaus, R. Bernotas, R. Unwalla, E. Quinet, D. Savio, A. Halpern, M. Basso, J. Keith, V. Clerin, L. Chen, Q.Y. Liu, I. Feingold, C. Huseilton, F. Azam, A. Goos-Nilsson, A. Wilhelmsson, P. Nambi, J. Wrobel, Further modification on phenyl acetic acid based quinolines as liver X receptor modulators, *Bioorg. Med. Chem.* 15 (2007) 3321–3333.
- [14] B. Hu, E. Quinet, R. Unwalla, M. Collini, J. Jetter, R. Dooley, D. Andracka, D. Nogle, L. Savio, A. Halpern, A. Goos-Nilsson, A. Wilhelmsson, P. Nambi, J. Wrobel, Carboxylic acid based quinolines as liver X receptor modulators that have LXRbeta receptor binding selectivity, *Bioorg. Med. Chem. Lett.* 18 (2008) 54–59.
- [15] B. Hu, R. Unwalla, M. Collini, E. Quinet, I. Feingold, A. Goos-Nilsson, A. Wilhelmsson, P. Nambi, J. Wrobel, Discovery and SAR of cinnolines/quinolines as liver X receptor (LXR) agonists with binding selectivity for LXRbeta, *Bioorg. Med. Chem.* 17 (2009) 3519–3527.
- [16] N.F. Valadares, L.B. Salum, I. Polikarpov, A.D. Andricopulo, R.C. Garratt, Role of halogen bonds in thyroid hormone receptor selectivity: pharmacophore-based 3D-QSSR studies, *J. Chem. Inf. Model.* 49 (2009) 2606–2616.
- [17] L.B. Salum, L.C. Dias, A.D. Andricopulo, Fragment-based QSAR and molecular modeling studies on a series of discodermolide analogs as microtubule-stabilizing anticancer agents, *QSAR Comb. Sci.* 28 (2009) 325–337.
- [18] K.M. Honorio, L.B. Salum, R.C. Garratt, I. Polikarpov, A.D. Andricopulo, Two- and three-dimensional quantitative structure–activity relationships studies on a series of liver X receptor ligands, *Open Med. Chem. J.* 2 (2008) 87–96.
- [19] K.C. Weber, K.M. Honorio, A.D. Andricopulo, A.B.F. da Silva, Two-dimensional QSAR studies on arylpiperazines as high-affinity 5-HT1A receptor ligands, *Med. Chem.* 4 (2008) 328–335.
- [20] M. Ye, Hologram QSAR studies of N,N-dialkyl-2-phenylindol-3-ylglyoxylamides derivatives as selective peripheral benzodiazepine receptor ligands, *Lett. Drug Des. Discov.* 7 (2010) 133–138.
- [21] K.C. Weber, F. de Lima, P.H. de Mello, A.B.F. da Silva, K.M. Honorio, Insights into the molecular requirements for the anti-obesity activity of a series of CB1 ligands, *Chem. Biol. Drug Des.* 76 (2010) 320–329.
- [22] T.S. Garcia, K.M. Honorio, Two-dimensional quantitative structure–activity relationship studies on bioactive ligands of peroxisome proliferator-activated receptor delta, *J. Braz. Chem. Soc.* 22 (2011) 65–72.
- [23] L.B. Salum, A.D. Andricopulo, Fragment-based QSAR: perspectives in drug design, *Mol. Divers.* 13 (2009) 277–285.
- [24] L.B. Salum, A.D. Andricopulo, Fragment-based QSAR strategies in drug design, *Expert Opin. Drug Discov.* 5 (2010) 405–412.
- [25] D.R. Lewis, HQSAR. A new, highly predictive QSAR technique, *Tripos Technical Notes*, vol. 1, 1997, pp. 1–7.
- [26] G. Klebe, U. Abraham, T. Mietzner, Molecular similarity indices in a comparative analysis (CoMSIA) of drug molecules to correlate and predict their biological activity, *J. Med. Chem.* 37 (1994) 4130–4146.
- [27] L.B. Salum, N.F. Valadares, Fragment-guided approach to incorporating structural information into a CoMFA study: BACE-1 as an example, *J. Comput. Aided Mol. Des.* 24 (2010) 803–817.
- [28] S. Williams, R.K. Bledsoe, J.L. Collins, S. Boggs, M.H. Lambert, A.B. Miller, J. Moore, D.D. McKee, L. Moore, J. Nichols, D. Parks, M. Watson, B. Wisely, T.M. Willson, X-ray crystal structure of the liver X receptor beta ligand binding domain: regulation by a histidine–tryptophan switch, *J. Biol. Chem.* 278 (2003) 27138–27143.